



CHORUS

This is the accepted manuscript made available via CHORUS. The article has been published as:

Effects of Al content and annealing on the phases formation, lattice parameters, and magnetization of $\text{Al}_{\{x\}}\text{Fe}_{\{2\}}\text{B}_{\{2\}}$ ($x=1.0,1.1,1.2$) alloys

E. M. Levin, B. A. Jensen, R. Barua, B. Lejeune, A. Howard, R. W. McCallum, M. J. Kramer, and L. H. Lewis

Phys. Rev. Materials **2**, 034403 — Published 26 March 2018

DOI: [10.1103/PhysRevMaterials.2.034403](https://doi.org/10.1103/PhysRevMaterials.2.034403)

Revised_12-23-2017

Effects of Al content and annealing on the phases formation, lattice parameters, and magnetization of $\text{Al}_x\text{Fe}_2\text{B}_2$ ($x = 1.0, 1.1, 1.2$) alloys

E. M. Levin,^{1,2*} B. A. Jensen,¹ R. Barua,³ B. Lejeune,³ A. Howard,¹
R. W. McCallum,⁵ M. J. Kramer,^{1,4} and L. H. Lewis³

¹ *Division of Materials Sciences and Engineering, U.S. Department of Energy Ames Laboratory, Ames, Iowa, USA*

² *Department of Physics and Astronomy, Iowa State University, Ames Iowa, USA*

³ *Department of Mechanical Engineering, Northeastern University, Boston, MA, USA*

⁴ *Department of Materials Sciences and Engineering, Iowa State University, Ames Iowa, USA*

⁵ *McCallum Consulting LLC, Santa Fe, NM, USA*

Submitted to *Physical Review Materials*

Abstract. AlFe_2B_2 is a ferromagnet with the Curie temperature around 300 K and has the potential to be an outstanding rare-earth free candidate for magnetocaloric applications. However, samples prepared from the melt contain additional phases which affect the functional response of the AlFe_2B_2 phase. We report on the effects of Al content in samples with the initial (nominal) composition of $\text{Al}_x\text{Fe}_2\text{B}_2$ where $x=1.0, 1.1,$ and 1.2 prepared by arc-melting followed by suction casting and annealing. The as-cast $\text{Al}_x\text{Fe}_2\text{B}_2$ alloys contain AlFe_2B_2 as well as additional phases including the primary solidifying FeB and $\text{Al}_{13}\text{Fe}_4$ compounds which are ferromagnetic and paramagnetic, respectively, at 300 K. The presence of these phases makes it difficult to extract the intrinsic magnetic properties of AlFe_2B_2 phase. Annealing of $\text{Al}_x\text{Fe}_2\text{B}_2$ alloys at 1040 °C for 3 days allows for reaction of the FeB with $\text{Al}_{13}\text{Fe}_4$ to form the AlFe_2B_2 phase, significantly reduces the amount of additional phases, and results in nearly pure AlFe_2B_2 phase as confirmed with XRD, magnetization, scanning electron microscopy, and electronic transport. The values of the magnetization, effective magnetic moment per Fe atom, specific heat capacity, electrical resistivity and Seebeck coefficient for the AlFe_2B_2 compound have been established.

Keywords: $\text{Al}_x\text{Fe}_2\text{B}_2$ alloys; suction casting; annealing; XRD, lattice parameters; SEM, EDS; DSC, magnetization, heat capacity, electrical resistivity, Seebeck coefficient.

* Corresponding author, E-mail: levin@iastate.edu

I. INTRODUCTION

The magnetocaloric effect, defined as heat release or absorption triggered by application and removal of a magnetic field [1], is anticipated for wide application in cooling devices [2]. If the magnetocaloric effect is large enough, it has the potential to be used in magnetic refrigeration. Large effects are observed in various materials including rare-earth alloys based on $\text{Gd}_5\text{Si}_2\text{Ge}_2$, $\text{La}(\text{Fe},\text{Si})_{13}$, as well as alloys based on MnAs and other compounds [1,3]. As cost and availability of materials is an important issue in refrigeration, the current goals are focused on developing novel high-efficiency magnetocaloric materials which do not contain expensive components such as rare-earth elements. Among such rare-earth-free materials, the ternary compound AlFe_2B_2 [4,5] has the potential to be a promising candidate for magnetocaloric applications [4-6].

The AlFe_2B_2 (1:2:2) ternary compound crystallizes in an orthorhombic space group $Cmmm$ and exhibits a Curie temperature close to room temperature [4-8]. In this crystal structure, the Fe atoms are bonded with B atoms and form atomic layers (slabs) constituting a predominantly two-dimensional magnetic system. The Curie temperature, T_C , of the AlFe_2B_2 phase can be modified by the replacement of Fe with Cr, Mn, Co, and Ni [6,9-12]. Understanding of exchange interactions between Fe magnetic moments in anisotropic magnetic systems like AlFe_2B_2 is a subject of great interest and is necessary to determine the potential of AlFe_2B_2 for magnetocaloric applications. However, the peritectic nature of the AlFe_2B_2 compound formation from the melt makes it difficult to synthesize the pure AlFe_2B_2 phase [6,9]. Additional phases form during solidification and contribute to the magnetization of these alloys making assessment of the intrinsic properties challenging.

The AlFe_2B_2 can be obtained by arc-melting of Al, Fe, and B mixture in the $N:2:2$ ratio, where N can vary from 1.5 to 3 [6,9]. In addition, Tan *et al.* [9] melted Al:Fe:B:Ga with the 1.5:1.8:2:10 ratio under Ga flux in an alumina crucible, whereas Du *et al.* [13] synthesized AlFe_2B_2 by melt spinning. ElMassalami *et al.* [4] and Tan *et al.* [9] reported that a significant amount of secondary binary phases including $\text{Al}_{13}\text{Fe}_4$ is present in alloys synthesized by arc-melting or by melting under Ga flux in an alumina crucible. It was also stated that decreasing the Al content in their mixture resulted in the formation of the undesirable FeB phase [9]. For alloys synthesized with a higher amount of excess Al, the resultant $\text{Al}_{13}\text{Fe}_4$ phase can be easily removed by treating with a dilute HCl acid; this procedure provides a higher concentration of AlFe_2B_2 but does not remove the FeB [9].

While $\text{Al}_{13}\text{Fe}_4$ is ferromagnetic at temperatures below 5 K [14], the presence of ferromagnetic FeB with the Curie temperature of ~ 590 K [15], significantly affects the room-temperature magnetization and magnetocaloric effect of the alloy. While the effect from the paramagnetic $\text{Al}_{13}\text{Fe}_4$ phase [14] is not significant, its presence reduces the contribution of AlFe_2B_2 and it is thus detrimental to extracting intrinsic parameters.

In this paper we analyze the effects of variation of the Al content in alloys with initial (nominal) composition of $\text{Al}_x\text{Fe}_2\text{B}_2$ with $x = 1.0, 1.1, \text{ and } 1.2$ on the phase purity, solidification structure, magnetic properties and **electronic** transport. Samples are made by suction casting from the melt and are studied in both the as-cast and annealed states.

It is demonstrated that the concentration of the FeB and $\text{Al}_{13}\text{Fe}_4$ phases, which coexist in as-cast alloys with the desired AlFe_2B_2 phase, can be significantly reduced via selection of the proper initial Al content combined with post-solidification annealing treatment. Starting with Al

enrichment of $x=1.2$ and annealing at $1040\text{ }^{\circ}\text{C}$, it is possible to obtain nearly pure AlFe_2B_2 material in significant amounts.

II. EXPERIMENTAL DETAILS

$\text{Al}_x\text{Fe}_2\text{B}_2$ alloys with $x = 1.0, 1.1$ and 1.2 (also can be shown as $\text{Al}:\text{Fe}:\text{B}$ with $N:2:2$ where $N = 1.0, 1.1, 1.2$) were synthesized using FeB and Al (99.999%). FeB was prepared by arc-melting of Fe (99.999%) and B (99.5%). Note that $\text{Al}_x\text{Fe}_2\text{B}_2$ chemical formula represents the initial (nominal) composition of alloys, whereas the phase of interest is AlFe_2B_2 . The FeB and Al starting materials were arc-melted, turned and re-melted several times for homogenization. Following this procedure, the ingots were subsequently suction-cast into a ~ 5 mm copper mold to insure the melt fully fills the mold thus making a fully dense, well quenched sample.

The resulting 15-g ingot was ~ 5 mm in diameter and ~ 60 mm in length; Figure 1 shows a typical ingot of the suction-cast $\text{Al}_x\text{Fe}_2\text{B}_2$ alloy, which was cut into smaller cylindrical pieces for measurements. For annealing, pieces of each ingot were wrapped with tantalum foil and sealed in a quartz ampoule, which was back filled to 0.3 atm with high purity argon. The ampoule was heated in a furnace from room temperature to the annealing temperature at $1040\text{ }^{\circ}\text{C}$ and held for 3 days. The annealing temperature was chosen on the basis of calorimetry measurements, described below. All samples were "furnace cooled" to $\sim 800\text{ }^{\circ}\text{C}$ over the course of 15 min and then water quenched.

In order to minimize the duration of the experiments, the samples are quenched into water upon reaching $800\text{ }^{\circ}\text{C}$. The effect of various cooling protocols were tested: (1) furnace cooling from $1040\text{ }^{\circ}\text{C}$ to room temperature, (2) quenching from $1040\text{ }^{\circ}\text{C}$ to room temperature and (3) quenching from $1040\text{ }^{\circ}\text{C}$ to $600\text{ }^{\circ}\text{C}$ and then annealing at $600\text{ }^{\circ}\text{C}$. Differences in samples

subjected to the heat treatment procedures were not detectable by either magnetization nor differential scanning calorimetry measurements.

Differential scanning calorimetry (DSC) measurements were performed with a Netzsch STA 409 PC at a heating rate of 20 K/min in pure helium. X-ray diffraction (XRD) patterns were obtained at 300 K from powdered samples using a Bruker diffractometer employing $\text{Cu-K}\alpha$ radiation ($\lambda = 0.1541$ nm). Lattice parameters were calculated using Rietveld refinements in the program X'Pert HighScore Plus [16]. The morphology and chemical compositions of the samples were assessed by scanning electron microscopy (SEM, FEI Teneo FE-SEM, operated at 10 kV/1.6 nA) with energy dispersive spectroscopy (SEM-EDS, Oxford Aztec system with X-Max 80 Silicon Drift Detector) attached to the Teneo. Multiple regions within a sample were assessed to determine variation in composition. The samples were compression mounted in a diallyl phthalate-mineral filled resin. The samples were polished to a mirror finish using silicon carbide grinding paper (grits 400, 600, and 800) and then using 6 μm and 1 μm diamond polishing paste on nylon.

The magnetization, M , of the as-cast and annealed $\text{Al}_x\text{Fe}_2\text{B}_2$ alloys was measured as a function of a magnetic field and temperature using a Physical Property Measurement System (PPMS), Dynacool, Quantum Design with the vibrating sample magnetometer (VSM) option. The measurements protocol was as follows: after a temperature increase from 300 K to 400 K in zero magnetic field, i.e. above the Curie temperature of AlFe_2B_2 , the M vs. H dependence was measured at 400 K in the field range between -90 and 90 kOe. After magnetic demagnetization, the M vs. T dependence was measured in a 20 kOe on cooling from 400 K to 50 K at a sweep rate of 2 K/min. Magnetization M vs. H data were collected at 50 K, and then after magnetic

demagnetization M vs. T dependence was measured in a 20 kOe magnetic field on heating from 50 K to 400 K. The relative error of the magnetization measurements was $\sim 2\%$.

The specific heat capacity was measured by the relaxation method [17] using the heat capacity option of a Quantum Design PPMS in the temperature range from 7 to 325 K in zero applied magnetic field; the error of heat capacity measurements is $\sim 1\%$. The electrical resistivity and Seebeck coefficient were measured in the temperature range of 20-400 °C using LSR-3 measuring system (Linseis, Inc.). Samples for electrical resistivity and Seebeck coefficient had a cylindrical shape with a diameter of 5.5 mm and a height of 12 mm. For measurements of the electrical resistivity, we used the four probe method with platinum electrodes. The temperature difference for the Seebeck effect measurements was ~ 8 °C; the relative errors of measurements are 3% and 5%, respectively (see more details in Ref. 18).

III. EXPERIMENTAL DATA AND DISCUSSION

3.1. Differential scanning calorimetry

In order to optimize the heat treatment and maximize the AlFe_2B_2 phase content in $\text{Al}_x\text{Fe}_2\text{B}_2$ alloys, we have examined as-cast samples using differential scanning calorimetry. The as-cast sample with initial composition of $\text{Al}_{1.2}\text{Fe}_2\text{B}_2$ demonstrates on heating (Fig. 2) three peaks with onset temperatures of 1030 °C, 1060 °C, and 1280 °C. Based on the phase composition of the as-cast sample (see discussion below), the peak at 1280 °C is attributed to the peritectic decomposition of the AlFe_2B_2 into FeB and liquid, whereas the low-temperature peaks are attributed to a ternary eutectic and another low melting temperature phase. The liquidus, where the FeB formed during the peritectic decomposition reaction, is not observed as it occurs above the range of measurements. It is clear that low-melting-temperature liquid must react with

the FeB to form the desired AlFe_2B_2 phase in single-phase form. DSC for the alloys with initial composition of $\text{Al}_{1.0}\text{Fe}_2\text{B}_2$ and $\text{Al}_{1.1}\text{Fe}_2\text{B}_2$ demonstrates similar behavior.

Phase segregation during annealing as a result of liquid migration may be avoided by employing an annealing temperature that is just below the lowest liquid formation temperature; Using this rationale, an annealing temperature of 1040 °C was chosen. The calorimetry data obtained for the $\text{Al}_{1.2}\text{Fe}_2\text{B}_2$ sample annealed at 1040 °C for 3 days (Fig. 2) confirmed that the phase that produced the lower melting temperature liquid had been consumed and the endothermic peak associated with the AlFe_2B_2 peritectic decomposition reaction has increased in magnitude, signaling the presence of an increased amount of the 1:2:2 phase.

3.2. XRD, phase content, and lattice parameters

Figure 3 show XRD patterns of samples with the initial composition of $\text{Al}_x\text{Fe}_2\text{B}_2$, where $x = 1.0$ [Fig. 3(a) and Fig. 3(b)] and 1.2 [Fig.3(c) and Fig. 3(d)], in the as-cast and annealed states. In the as-cast state the alloys contain 66-72 wt.% of the AlFe_2B_2 phase along with two additional phases, FeB and $\text{Al}_{13}\text{Fe}_4$ (Table 1). The amount of ferromagnetic FeB phase, which can mask the intrinsic magnetic properties of AlFe_2B_2 , decreases from 20 to 11 wt.% with increased Al content. The amount of paramagnetic $\text{Al}_{13}\text{Fe}_4$ phase in as-cast alloys is determined to be between 13 and 17 wt.%. Annealing at 1040 °C for 3 days significantly reduces the fractions of secondary phases and increases the AlFe_2B_2 content: $\text{Al}_{1.0}\text{Fe}_2\text{B}_2$ and $\text{Al}_{1.2}\text{Fe}_2\text{B}_2$ alloys contain 97.7 wt.% and ~100 wt.%, respectively. XRD data for as-cast and annealed alloy with the initial composition of $\text{Al}_{1.1}\text{Fe}_2\text{B}_2$ confirm this trend (Table 1).

The lattice parameters determined for the AlFe_2B_2 phase in $\text{Al}_x\text{Fe}_2\text{B}_2$ alloys in this study are very similar to those reported by Tan *et al.* [9] for samples prepared by arc-melting. After

annealing at 1040 °C for 3 days, the fraction of FeB and Al₁₃Fe₄ phases present in the Al_{1.0}Fe₂B₂ and Al_{1.1}Fe₂B₂ decreases, whereas no secondary phases are detected in Al_{1.2}Fe₂B₂ alloy, within the detectable limits of XRD. Our data demonstrate that selection of the proper Al enrichment combined with high-temperature annealing enables achievement of nearly single-phase AlFe₂B₂ material. We suggest that using optimal Al content and annealing temperature, duration of the annealing time can be significantly reduced, but this requires additional study. A lack of any significant change in lattice parameters indicates that there is little or no variability in the 1:2:2 compositional ratio in all samples studied here.

Based on the DSC and X-ray diffraction data, the portion of the ternary phase diagram in the vicinity of AlFe₂B₂ has been estimated (Fig. 4). The AlFe₂B₂ compound is confirmed to form by a peritectic reaction with limited range of solid solutions. This solid solution may extend partially out of the plane of this 2D cut through the ternary diagram. However, the exact range of solid solution has not been determined and may be minimal based on EDS data and minimal changes in the lattice parameters discussed below. Formation of microscopic FeB cannot be avoided when the alloy solidified through this two-phase region, which extends over 200 °C at the cooling rates available during standard arc-melting.

3.3. Microstructure and composition

Scanning electron microscopy (SEM) and energy dispersive spectroscopy (EDS) were used to understand the processing-induced evolution of the morphology and composition of the alloys with initial composition of Al_{1.1}Fe₂B₂ and Al_{1.2}Fe₂B₂ containing a small fraction of ferromagnetic FeB phase. Backscattering SEM images of Al_{1.1}Fe₂B₂ in the as-cast and annealed forms [Fig.5(a) and Fig. 5(b)] demonstrate the effects of annealing. As-cast samples show

dendrite-like features with a small amount of eutectic microstructure existing between the dendrite arms.

The dendrites with approximate dimensions between 3 and 10 μm appear at different gray contrast levels in the image, indicating that they have different compositions. A dendrite-like structure in an arc-melted AlFe_2B_2 alloy has been reported by Hirt *et al.* [6]. The authors prepared this 1:2:2 alloy using spark plasma sintering (SPS), but the SPS samples still contained additional phases which affect the properties of the alloy.

Images of the alloy of initial composition of $\text{Al}_{1.2}\text{Fe}_2\text{B}_2$ are shown in Fig.5(c) and Fig.5(d). It is observed that an increase in the Al content in this alloy results in the appearance of larger dendrites; heat treatment promotes the formation of the desired dense, large-grained single-phase AlFe_2B_2 alloy. The composition of the $\text{Al}_{1.2}\text{Fe}_2\text{B}_2$ as-cast and annealed alloys was assessed from several points on the surface of both samples. EDS data obtained in several points for the annealed alloys with the initial composition of $\text{Al}_{1.1}\text{Fe}_2\text{B}_2$ and $\text{Al}_{1.2}\text{Fe}_2\text{B}_2$ shows that the Al:Fe ratios are 0.43 and 0.46, respectively, which is slightly smaller compared to the 0.5 value expected for the 1:2:2 stoichiometric compound. Since boron is difficult to quantify, the Al:Fe ratio is a more reliable measure of the stoichiometry and suggests site exchange for Al and Fe.

These results indicate that the light-contrast dendrites have approximate composition of FeB containing small amount of aluminum, ~ 1.4 at.%, while gray-contrast dendrites have the approximate composition close to AlFe_2B_2 , and the dark dendrites are the $\text{Al}_{13}\text{Fe}_4$ phase, containing some boron. After annealing, the dendritic structure of this sample also disappears, and the material contains large grains with uniform contrast indicative of predominately pure AlFe_2B_2 phase with a much smaller amount of second phase resident on the grain boundaries.

Because melting temperature of Al, 660 °C, is much lower compared to that of Fe, 1538 °C, and B, 2076 °C, some of the Al can be lost throughout the processing, so excess aluminum is needed. The losses of aluminum are expected for a number of reasons: evaporation during the arc-melting process and removal of the quenched eutectic liquid from the top of the ingot after the suction casting process. Annealing also results in some loss of excess Al during transformation of $\text{Al}_{13}\text{Fe}_4$ and FeB phases to AlFe_2B_2 phase. This phase transformation is accompanied by the appearance of an Al-rich liquid which migrates by capillary motion to surface of the ingot, wetting the surface of the Ta foil.

3.4. Magnetic field and temperature dependencies of magnetization

Because all $\text{Al}_x\text{Fe}_2\text{B}_2$ arc-melted suction cast alloys contain ferromagnetic FeB (Table 1), which definitely affects their magnetic properties, magnetization data for this compound is important and enables to estimate its fraction in each sample. The magnetization of FeB measured by us in a 20 kOe magnetic field is 95.6 and 74.9 emu/g at 50 and 400 K, respectively, which is significantly larger than that of AlFe_2B_2 (see Refs. 4,6,9 and Table 2); the saturation magnetization of FeB is observed in magnetic field about 6 kOe, which is less than that of $\text{Al}_x\text{Fe}_2\text{B}_2$ alloys (see below). The Curie temperature of our FeB sample, 590 K, is similar to that reported by Rades *et al.* [15], and is much higher than that of AlFe_2B_2 . The phase fraction of FeB in the samples as deduced from XRD data can be confirmed using the measured magnetization of the synthesized FeB.

The magnetization vs. applied magnetic field for the as-cast and annealed $\text{Al}_x\text{Fe}_2\text{B}_2$ alloys measured at 50 K and 400 K are shown in Fig. 6. Magnetization of all as-cast alloys at 50 K is very similar [Fig. 6(a)] whereas each alloy contains secondary FeB and $\text{Al}_{13}\text{Fe}_4$ phases (Table 1).

This demonstrates that the contribution from the major and secondary phases cannot be distinguished and measured magnetization at 50 K may not be used for estimation of the AlFe_2B_2 phase fraction.

In contrast, low-magnetic field saturation magnetization of all alloys observed at 400 K clearly demonstrates the presence of FeB phase; the fraction of this phase gradually reduces when Al content increases which agrees well with XRD data. A comparison of the magnetization values in as-cast alloys measured at 400 K in a 20 kOe magnetic field with those calculated from the FeB content obtained from XRD shows good agreement (Table 2). The contribution from $\text{Al}_{13}\text{Fe}_4$ phase, which is paramagnetic above 5 K [14], in all alloys is small.

After annealing, the values of the magnetization of $\text{Al}_x\text{Fe}_2\text{B}_2$ alloys at 50 K are slightly different reflecting the difference in content of secondary phases.

Larger value of the magnetization of $\text{Al}_{1.0}\text{Fe}_2\text{B}_2$ compared to that of $\text{Al}_{1.1}\text{Fe}_2\text{B}_2$ and $\text{Al}_{1.2}\text{Fe}_2\text{B}_2$ can be attributed to the presence of FeB phase. At 400 K, the values of the magnetization are much smaller [Fig. 6(b) and Table 2] compared to those of as-cast alloys indicating that the amount of ferromagnetic FeB phase is significantly reduced. The annealed $\text{Al}_{1.0}\text{Fe}_2\text{B}_2$ sample exhibits a very small ferromagnetic contribution present in the 400 K hysteresis loop that is attributed to 2.3 wt.% of FeB. However, M vs. H data obtained at 400 K for the $\text{Al}_{1.1}\text{Fe}_2\text{B}_2$ and $\text{Al}_{1.2}\text{Fe}_2\text{B}_2$ samples do not show any additional ferromagnetic FeB phase. Furthermore, the annealed $\text{Al}_{1.2}\text{Fe}_2\text{B}_2$ alloy does not contain the $\text{Al}_{13}\text{Fe}_4$ phase (Table 1); thus this sample may be considered to be phase-pure and can be used for characterization of the intrinsic properties of the AlFe_2B_2 compound. M vs. H dependencies for $\text{Al}_x\text{Fe}_2\text{B}_2$ alloys demonstrate very small coercive force, a few oersted, which is an advantage for magnetocaloric

materials. The approach to saturation of all annealed samples is nonlinear even up to higher fields, consistent with the presence of appreciable magnetocrystalline anisotropy.

Figure 7 demonstrates M vs. T dependencies measured on heating in a 20 kOe magnetic field for as-cast and annealed $\text{Al}_x\text{Fe}_2\text{B}_2$ alloys after they were magnetically demagnetized; similar dependencies were observed for measurements on cooling. Similar to M vs. H , M vs. T dependencies are typical for a second order ferromagnet to paramagnet transition. The value of the magnetization at temperatures above T_C reduces with an increase of Al amount, which supports XRD data and shows that Al excess results in formation of smaller fraction of FeB phase. A major effect of annealing is observed in the vicinity of the ferromagnet - paramagnet transition, where the magnetization of annealed samples demonstrates sharper transition.

It is well known that the magnetic susceptibility, χ , of ferromagnetic materials at temperatures above T_C can be described by the Curie law $\chi = M/H = C/(T-T_C)$ where C is the Curie constant. Above T_C , the H/M vs. T dependence can be approximated by line, so at $H/M = 0$ $T - T_C = 0$, which enable to estimate T_C : Using this approach for annealed $\text{Al}_x\text{Fe}_2\text{B}_2$ alloys and the data for $T > 310$ K (Fig. 8), we calculated the value of T_C : 293 K for $\text{Al}_{1.0}\text{Fe}_2\text{B}_2$ and 282 K for both $\text{Al}_{1.1}\text{Fe}_2\text{B}_2$ and $\text{Al}_{1.2}\text{Fe}_2\text{B}_2$. The latter value for AlFe_2B_2 compound is similar to that reported by Chai *et al.* [10], but is lower than $T_C = 290$ K reported by Hirt *et al.* [6]. The higher T_C value determined for the $\text{Al}_{1.0}\text{Fe}_2\text{B}_2$ is attributed to the influence of the appreciable FeB content in this sample. It is likely that the high T_C reported by Hirt *et al.* [6], as well as even higher $T_C = 320$ K value reported by ElMassalami *et al.* [4], may also be explained by the presence of FeB in the samples.

As the annealed $\text{Al}_{1.2}\text{Fe}_2\text{B}_2$ alloy is assessed, within the limits of detection, to be pure AlFe_2B_2 phase, magnetic data for this sample can be used to determine the Curie temperature and

the effective magnetic moment per Fe atom. The magnetic susceptibility of $\text{Al}_{1.2}\text{Fe}_2\text{B}_2$ at 400 K is 6.45×10^{-5} emu/(g Oe) and the calculated effective magnetic moment per Fe atom is $1.56 \mu_{\text{B}}$. This value is larger than that reported by Tan *et al.*, 1.15 and $1.03 \mu_{\text{B}}$ per Fe atom, obtained from the saturation magnetization at 1.8 K for alloys prepared by arc-melting and under Ga flux, respectively [9].

3.5. Specific heat capacity

The temperature dependencies of zero-magnetic field specific heat capacity, C_p , of annealed $\text{Al}_{1.0}\text{Fe}_2\text{B}_2$, $\text{Al}_{1.1}\text{Fe}_2\text{B}_2$, and $\text{Al}_{1.2}\text{Fe}_2\text{B}_2$ alloys are shown in Fig. 9. Peaks in C_p are observed for all three samples, which can be attributed to ferromagnet - paramagnet transition and reflect the change in the entropy due to magnetic order - disorder transition, as is observed in intermetallic ferromagnetic compounds containing transition elements [19] or in Gd metal [20].

The peak temperature of the phase-pure $\text{Al}_{1.2}\text{Fe}_2\text{B}_2$ sample of 271 K is identified with the magnetic phase transition in AlFe_2B_2 phase; the value of C_p peak is 124 J/mol K. The peak of $C_p = 120$ J/mol K for $\text{Al}_{1.1}\text{Fe}_2\text{B}_2$ is observed at slightly lower temperature of 268 K. In contrast, the C_p peak for $\text{Al}_{1.0}\text{Fe}_2\text{B}_2$ of 124 J/mol K is observed at higher temperature of 280 K, which can be explained by the presence of ferromagnetic phase FeB with T_C higher than that of $\text{Al}_{1.2}\text{Fe}_2\text{B}_2$. The C_p peak is also wider, which also can be attributed to the presence of FeB. Note that all values of C_p were found at the peak in C_p vs. T.

Our data demonstrate that the value of the heat capacity in $\text{Al}_{1.2}\text{Fe}_2\text{B}_2$ is 123 J/mol K, slightly larger compared to that reported by Tan *et al.* [9], 118 J/mol K. It should be noted that the values of room temperature C_p of well-known magnetocaloric materials [1], Gd, $\text{La}(\text{Fe},\text{Si})_{13}$ [1], and $\text{MnFeP}_{0.45}\text{As}_{0.55}$ [21] are ~ 50 J/mol K, ~ 900 J/mol K, and ~ 260 J/mol K, respectively.

One of the requirements for C_p of magnetocaloric materials is small specific heat capacity [1,22]; the value of C_p for AlFe_2B_2 is larger than that of Gd, but much smaller compared to that of $\text{La}(\text{Fe,Si})_{13}$ and $\text{MnFeP}_{0.45}\text{As}_{0.55}$.

3.6. Electrical resistivity and Seebeck coefficient

The value of the electrical resistivity is important for phase identity in general as well as a parameter that affects the energy dissipation and efficiency during magnetic cooling operations. The electrical resistivity and thermal conductivity in metallic systems are connected via the Wiedemann-Frantz law, illustrating that the magnitude of electrical resistivity is diagnostic of the potential magnitude of thermal transport [23]. Further, the Seebeck coefficient of metallic and semiconductor materials is very sensitive to the free charge carrier concentration and electronic states near the Fermi level, and thus they can be used as an independent signature of phase purity.

Figure 10(a) displays the temperature trends of electrical resistivity, ρ , and Seebeck coefficient, S , of as-cast $\text{Al}_{1.1}\text{Fe}_2\text{B}_2$ and $\text{Al}_{1.2}\text{Fe}_2\text{B}_2$ alloys. The electrical resistivity of both samples increases with increasing temperature, which is typical for metallic materials with high free carrier concentration [23]. The value of the electrical resistivity at 30 °C of as-cast $\text{Al}_{1.1}\text{Fe}_2\text{B}_2$ and $\text{Al}_{1.2}\text{Fe}_2\text{B}_2$ samples are 2.1 and 1.6 $\mu\Omega\text{-m}$, respectively, indicating that a higher Al content in the samples results in lower resistivity.

Electrical resistivity and Seebeck coefficient of annealed $\text{Al}_{1.1}\text{Fe}_2\text{B}_2$ and $\text{Al}_{1.2}\text{Fe}_2\text{B}_2$ alloys are shown in Fig. 10(b). The difference between the values of ρ is similar to that observed for as-cast samples, but the absolute value increase; the Seebeck coefficient of annealed alloys merge. At the current time it is not clear if this difference in the electrical resistivity values are intrinsic

(reflecting carrier concentration and mobility) or extrinsic (attributed to secondary phases and defects, including cracks); however, it is likely that both contributions affect electrical resistivity. These determined values are about one order of magnitude lower than that of the well-known magnetocaloric material $\text{Gd}_5\text{Ge}_2\text{Si}_2$, $\sim 20 \mu\Omega\text{-m}$ at 300 K [24], $\text{La}(\text{Fe},\text{Si})_{13}$, between 1.4 and 1.6 $\mu\Omega\text{-m}$ [25], and MnAs , between 1 and 10 $\mu\Omega\text{-m}$ [26]. Note that $\text{Gd}_5\text{Si}_2\text{Ge}_2$ and MnAs materials shows increase of electrical resistivity due to appearance of microcracks during passing through the first order magneto-structural phase transition [24,26].

While low electrical resistivity can result in energy dissipation and self-heating through eddy current driven by magnetic flux changes in the system operating at frequencies below 10 Hz, such as current MCE refrigeration prototypes, this effect is insignificant. However, low electrical resistivity is accompanied by an appreciable and advantageous thermal conductivity from free charge carriers, resulting in faster thermal response and a more intense heat exchange between the material and the heat-transfer fluid [1]. This is one of distinct advantages of AlFe_2B_2 material.

The Seebeck coefficient in electrically conductive materials is very sensitive to electronic states near the Fermi level, depends on free carrier concentration, and may adopt a wide range of values $\sim 5 \mu\text{V/K}$ in metals to $\sim 200 \mu\text{V/K}$ in semiconductors. The small measured values of the Seebeck coefficient of annealed $\text{Al}_{1.1}\text{Fe}_2\text{B}_2$ and $\text{Al}_{1.2}\text{Fe}_2\text{B}_2$ samples, $-25 \mu\text{V/K}$ at $\sim 300 \text{ K}$ [Fig.10(b)], are consistent with relatively low electrical resistivity.

IV. CONCLUSIONS

The effects of Al content and annealing on the phase formation, crystal structure, microstructure, magnetization, electrical resistivity and Seebeck coefficient of three $\text{Al}_x\text{Fe}_2\text{B}_2$

alloys with the initial (nominal) composition of $\text{Al}_{1.0}\text{Fe}_2\text{B}_2$, $\text{Al}_{1.1}\text{Fe}_2\text{B}_2$ and $\text{Al}_{1.2}\text{Fe}_2\text{B}_2$ prepared by arc-melting followed by suction casting have been studied. In the as-cast state, all alloys contain the major phase, AlFe_2B_2 , and two secondary phases, FeB , and $\text{Al}_{13}\text{Fe}_4$. In the as-cast $\text{Al}_x\text{Fe}_2\text{B}_2$ alloys, an increase in the initial Al content from 20 at.% to 23 at.% increases the amount of AlFe_2B_2 phase from 66.6 to 71.5 wt. % whereas the fraction of FeB decrease from 20.1 wt.% to 11.1 wt.% for $x = 1.0$ and 1.2, respectively.

The presence of ferromagnetic FeB with $T_C = 590$ K, which is much higher than that of AlFe_2B_2 , $T_C = 282$ K, affects magnetization of alloys at 50 K and particularly at 400 K. Annealing the $\text{Al}_x\text{Fe}_2\text{B}_2$ alloys at 1040 °C for 3 days reduces the fraction of ferromagnetic FeB in $\text{Al}_{1.0}\text{Fe}_2\text{B}_2$ and totally eliminates it in $\text{Al}_{1.1}\text{Fe}_2\text{B}_2$ and $\text{Al}_{1.2}\text{Fe}_2\text{B}_2$ samples; annealing also eliminate the paramagnetic $\text{Al}_{13}\text{Fe}_4$ phase in the $\text{Al}_{1.2}\text{Fe}_2\text{B}_2$ sample. Hence, the magnetic properties of the annealed sample with the initial composition of $\text{Al}_{1.2}\text{Fe}_2\text{B}_2$ are determined only by the AlFe_2B_2 phase itself. Our data demonstrate that pure AlFe_2B_2 material in significant amount can be obtained by arc-melting followed by suction casting and annealing for appropriate Al content without etching, which allows us to measure the intrinsic properties of AlFe_2B_2 phase.

ACKNOWLEDGEMENTS

Authors thank M. Lynn and W. Straszheim for SEM and EDA analysis. This work was conducted under the auspices of the Advance Research Projects – Energy (DE-AR0000754), US Department of Energy (DOE). The research was performed at the Ames Laboratory, which is operated for the U.S. Department of Energy by Iowa State University under Contract No DE-AC02-07CH11358, and in Northeastern University.

- [1] A. Kitanovski, J. Tusek, U. Tomc, U. Plaznik, M. Ozbolt, and A. Poredos. *Magnetocaloric Energy Conversion*. Springer, 456 p. (2015).
- [2] M. Liu and B. F. Yu. *J. Cent. South Univ. Technol.* **16**, 0001 (2009).
- [3] S. Fujieda, Y. Hasegawa, A. Fujita, and K. Fukamichi. *J. Appl. Phys.* **95**, 2429 (2004).
- [4] M. ElMassalami, D. da S. Olivera, and H. Takeya. *J. Magn. Magn. Mater.* **323**, 2133 (2011).
- [5] L. H. Lewis, R. Barua, and B. Lejeune. *J. Alloys and Comp.* **650**, 482 (2015).
- [6] S. Hirt, F. Yuan, Y. Mozharivsky, and H. Hillebrecht. *Inorganic Chemistry* **55**, 9677 (2016).
- [7] W. Jeitschko. *Acta Crystallogr. Sect. B: Struct. Crystallogr. Cryst. Chem.* **25**, 163 (1969).
- [8] Y. B. Kuz'ma and N. F. Chaban. *Inorg. Mater.* **5**, 321 (1969).
- [9] X. Tan, P. Chai, C. M. Thompson, and M. Shatruk. *J. Amer. Chem. Soc.* **135**, 9553 (2013).
- [10] P. Chai, S. A. Stoian, X. Tan, P. A. Dube, and M. Shatruk. *J. Solid State Chem.* **224**, 52 (2015).
- [11] Q. Du, G. Chen, W. Yang, J. Wei, M. Hua, H. Du, C. Wang, S. Liu, J. Han, Y. Zhang, and J. Yang. *J. Phys. D: Appl. Phys* **48**, 335001 (2015).
- [12] K. Kadas, D. Iusan, J. Hellsvik, J. Cedervall, P. Berastegui, M. Sahlberg, U. Jansson, and O. Erikson. *J. Phys.: Condens. Matter.* **29**, 155402 (2017).
- [13] Q. Du, G. Chen, W. Yang, Z. Song, M. Hua, H. Du, C. Wang, S. Liu, J. Han, Y. Zhang, and J. Yang. *Jap. J. Appl. Phys.* **54**, 053003 (2015).
- [14] P. Popcevic, A. Smontara, J. Ivkov, M. Wenska, M. Komeli, P. Jeglic, S. Vrtnik, M. Bobnar, Z. Jaglicic, B. Bauer, P. Gille, H. Borrmann, U. Burkhardt, Yu. Grin, and J. Dolinsek. *Physical Review B* **81**, 184203 (2010).
- [15] S. Rades, S. Kraemer, R. Seshadri, and B. Albert. *Chem.Mater.* **26**, 1549 (2014).
- [16] E. M. Levin, M. F. Besser, and R. Hanus *J. Appl. Phys.* **114**, 083713 (2013)

- [17] J. S. Hwang, K. J. Lin, and C. Tien. *Rev. Sci. Instrum.* **68**, 941 (1997).
- [18] E. M. Levin, S. L. Budko, and K. Schmidt-Rohr. *Adv. Funct. Mater.* **22**, 2766 (2012).
- [19] C. Pique, J. A. Blanco, R. Burriel, E. Abad, J. Fernandez-Rodriguez, and M. Artigas. *J. Phys. Condens. Matter.* **20**, 345203 (2008).
- [20] G. Bednarz. *Phys. Rev.* **47**, 14247 (1993).
- [21] O. Tegus, J. Klaasse, D. Thanh, W. Dagula, E. Bruck, K. Buschow, and F. De Boer. A specific-heat study of the phase transition in $\text{MnFeP}_{0.45}\text{As}_{0.55}$ compound. INTERMAG Conference, San Diego, p. 670-671 (2006).
- [22] M. H. Phan and S. C. Yu. *J. Magn. Magn. Mater.* **308**, 325 (2007).
- [23] G. J. Snyder and E. S. Toberer. *Nature Materials* **7**, 105 (2008).
- [24] E. M. Levin, V. K. Pecharsky, and K. A. Gschneidner, Jr. *Phys. Rev. B* **60**, 7993 (1999).
- [25] T. T. M. Palstra, J. A. Mydosh, G. J. Nieuwenhuys. *J. Magn. Magn. Mater.* **36** 290 (1983)
- [26] S. Haneda, N. Kazama, Y. Yamaguchi, and H. Watanabe. *J. Phys. Soc. Jpn.* **42**, 1201 (1977).



FIG. 1. A typical 15-g, ~5-mm in diameter ingot of $\text{Al}_x\text{Fe}_2\text{B}_2$ alloys synthesized by arc-melting followed by suction casting.

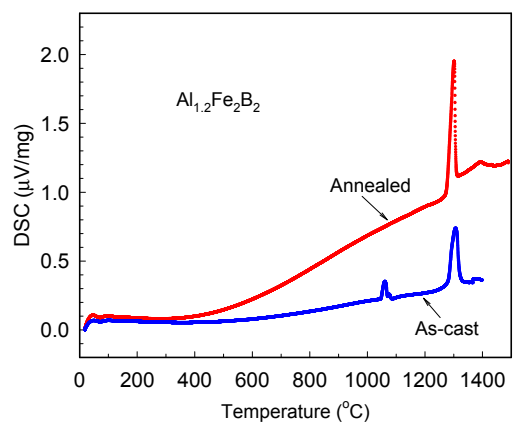


FIG. 2. Differential scanning calorimetry (DSC) of the alloy with the initial (nominal) composition of $\text{Al}_{1.2}\text{Fe}_2\text{B}_2$ as-cast and annealed at 1040 $^{\circ}\text{C}$ for 3 days measured on heating.

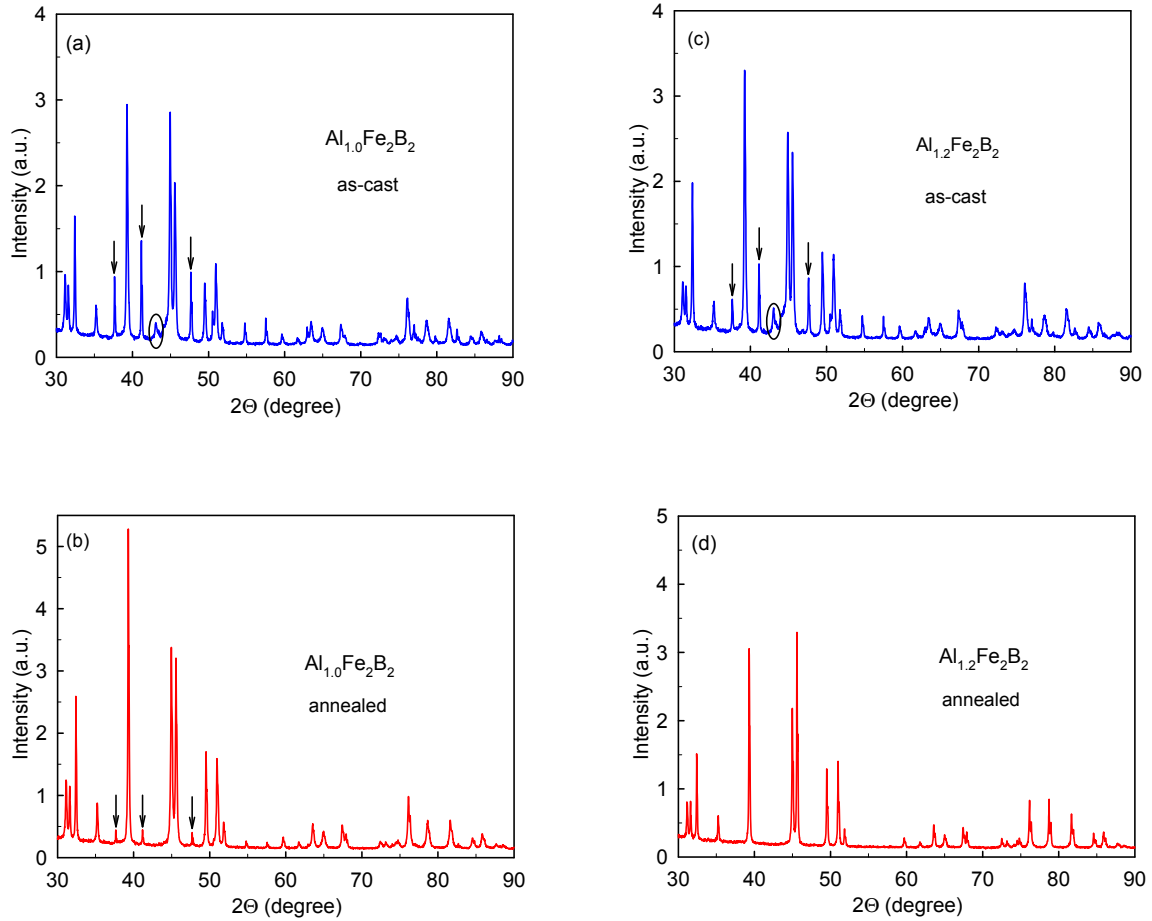


FIG. 3. XRD ($\text{Cu-K}\alpha$, $\lambda = 0.1541 \text{ nm}$) patterns of alloys with the initial (nominal) composition of $\text{Al}_{1.0}\text{Fe}_2\text{B}_2$ (a) as-cast and (b) annealed, and $\text{Al}_{1.2}\text{Fe}_2\text{B}_2$ (c) as-cast and (d) annealed. Arrows indicate peaks associated with FeB phase and ellipses indicate a peak associated with $\text{Al}_{13}\text{Fe}_4$ phase.

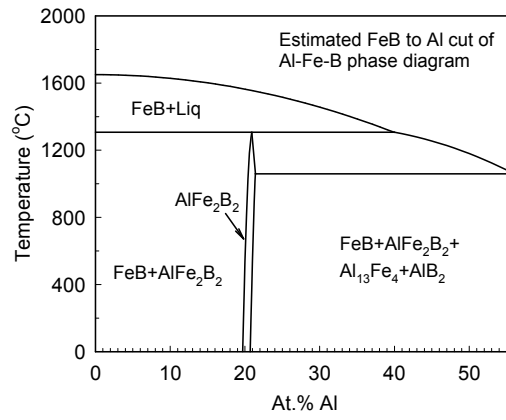


FIG. 4. Pseudo binary cut through the ternary Al-Fe-B phase diagram along the FeB to Al line; horizontal axis shows the at.% of Al in FeB.

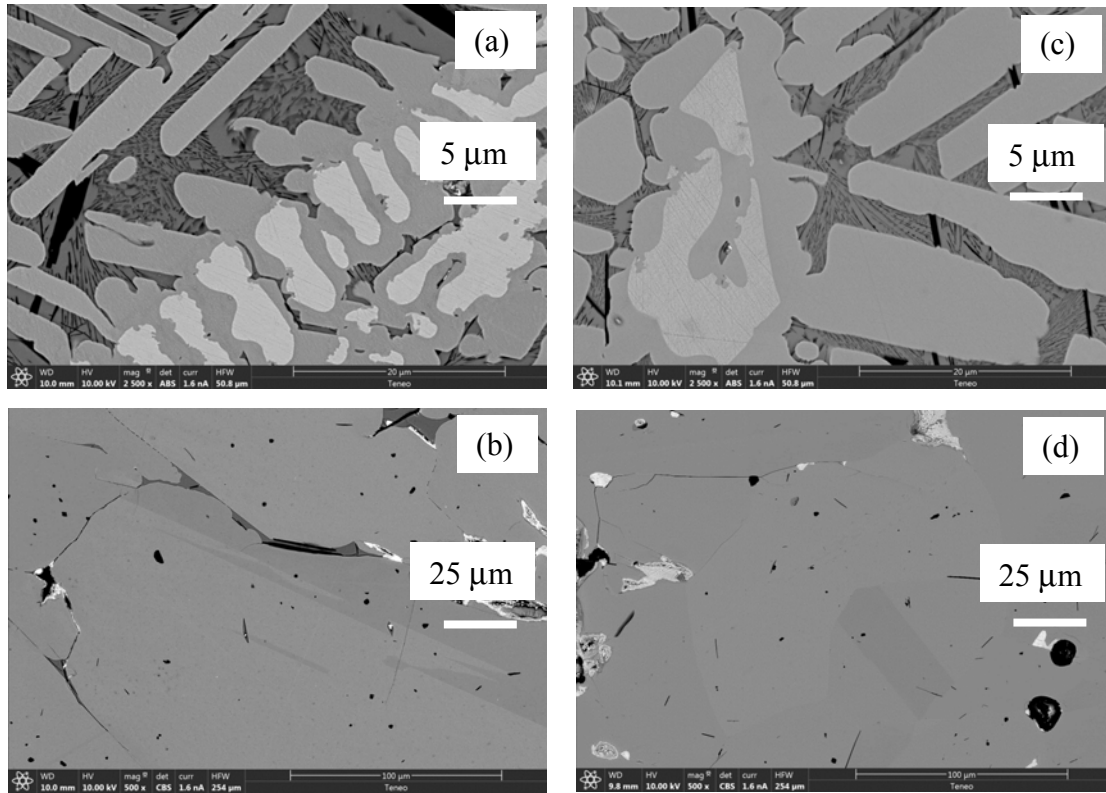


FIG. 5. Backscattered electron images of alloy with the initial (nominal) composition of $\text{Al}_{1.1}\text{Fe}_2\text{B}_2$ (a) as-cast, $\times 2500$, and (b) annealed, $\times 500$, and $\text{Al}_{1.2}\text{Fe}_2\text{B}_2$ (c) as-cast, $\times 2500$, and (d) annealed, $\times 500$.

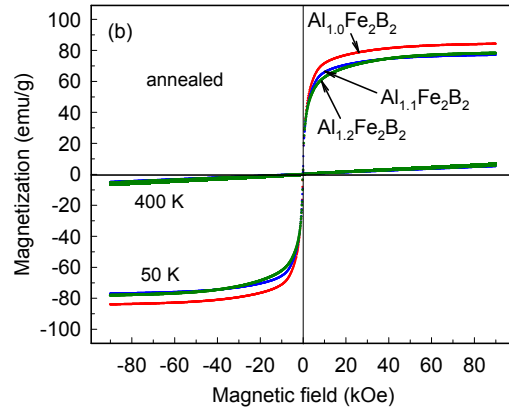
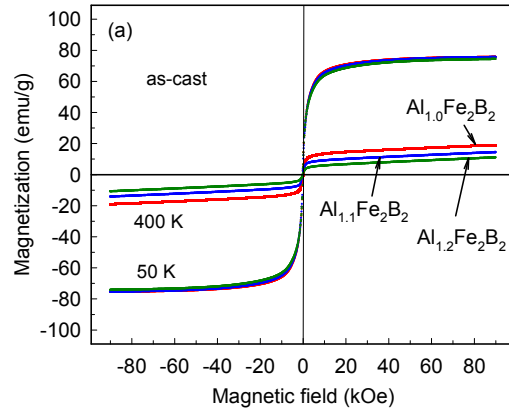


FIG. 6. Magnetization of (a) as-cast and (b) annealed alloys with the initial (nominal) composition of $\text{Al}_{1.0}\text{Fe}_2\text{B}_2$, $\text{Al}_{1.1}\text{Fe}_2\text{B}_2$, and $\text{Al}_{1.2}\text{Fe}_2\text{B}_2$ vs. magnetic field at 50 K and 400 K.

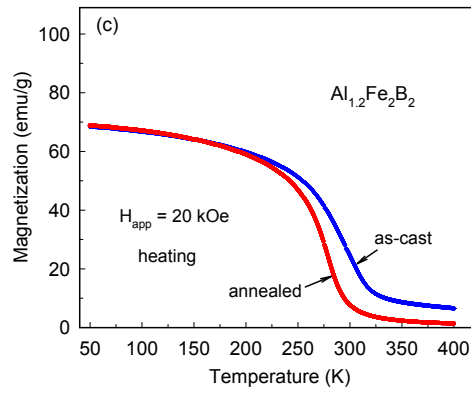
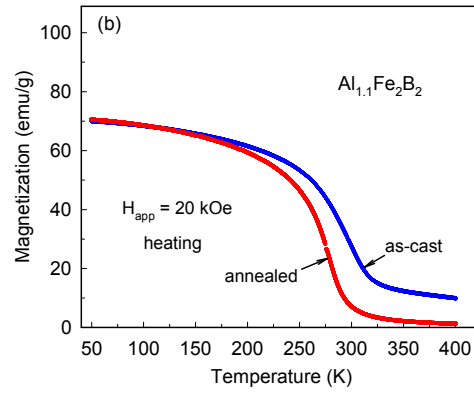
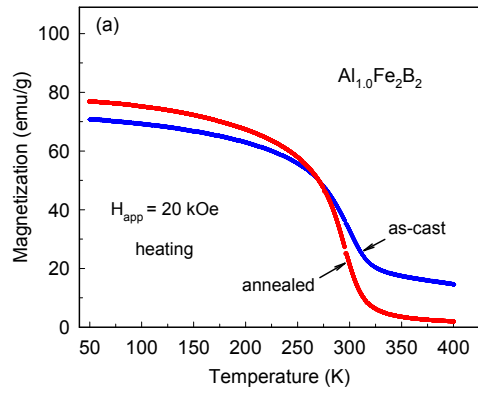


FIG. 7. Temperature dependencies of the magnetization of as-cast and annealed alloys with the initial (nominal) composition (a) $\text{Al}_{1.0}\text{Fe}_2\text{B}_2$, (b) $\text{Al}_{1.1}\text{Fe}_2\text{B}_2$, and (c) $\text{Al}_{1.2}\text{Fe}_2\text{B}_2$ samples measured in 20 kOe magnetic field.

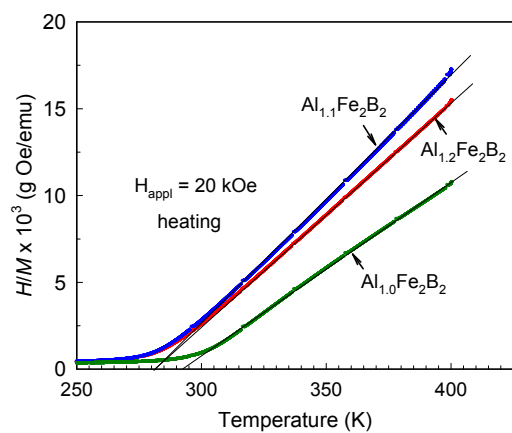


FIG. 8. Temperature dependence of the H/M ratio for alloys with the initial (nominal) composition of $Al_{1.0}Fe_2B_2$, $Al_{1.1}Fe_2B_2$, and $Al_{1.2}Fe_2B_2$ alloys annealed at 1040 °C for 3 days and measured in 20 kOe applied magnetic field on heating.

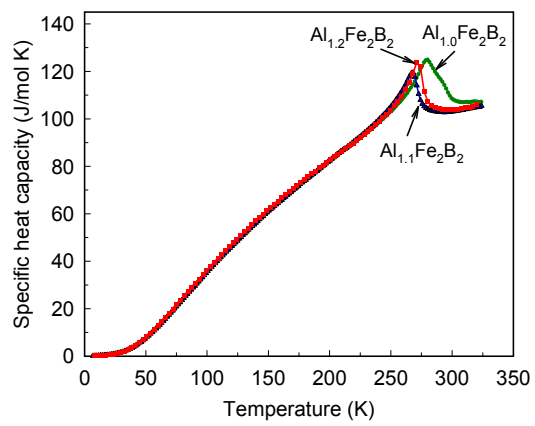


FIG. 9. Temperature dependencies of zero-magnetic field specific heat capacity for alloys with the initial (nominal) composition of $\text{Al}_{1.0}\text{Fe}_2\text{B}_2$, $\text{Al}_{1.1}\text{Fe}_2\text{B}_2$, and $\text{Al}_{1.2}\text{Fe}_2\text{B}_2$ annealed at $1040\text{ }^\circ\text{C}$ for 3 days.

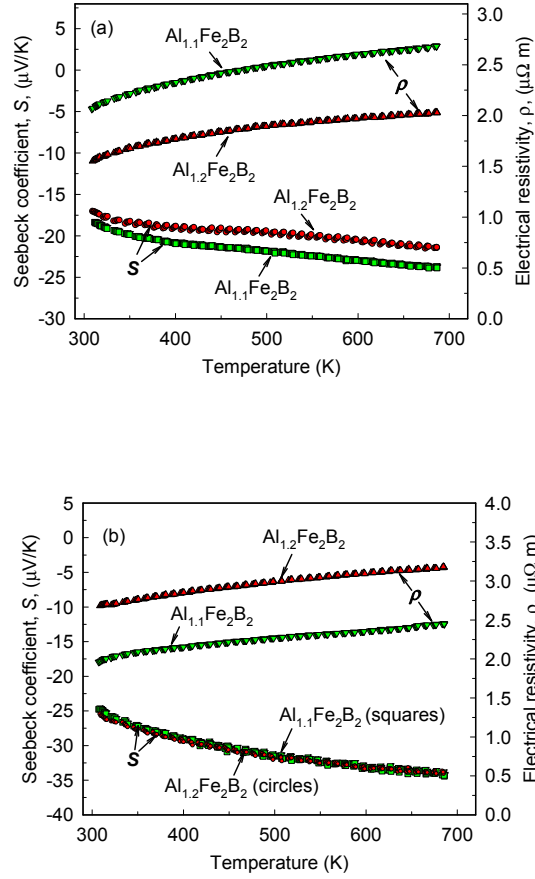


FIG. 10. Temperature dependencies of the electrical resistivity and Seebeck coefficient of alloys with the initial (nominal) composition of $\text{Al}_{1.1}\text{Fe}_2\text{B}_2$ and $\text{Al}_{1.2}\text{Fe}_2\text{B}_2$ (a) as-cast and (b) annealed at 1040 °C for 3 days.

Table 1.

Phases formed in as-cast and annealed alloys with initial compositions of $\text{Al}_x\text{Fe}_2\text{B}_2$, $x=1.0, 1.1,$ and $1.2,$ and their lattice parameters.

Phases formed in ingot and lattice parameters	$\text{Al}_{1.0}\text{Fe}_2\text{B}_2$		$\text{Al}_{1.1}\text{Fe}_2\text{B}_2$		$\text{Al}_{1.2}\text{Fe}_2\text{B}_2$	
	Phase content and lattice parameters		Phase content and lattice parameters		Phase content and lattice Parameters	
	as-cast	1040 °C 3 days	as-cast	1040 °C 3 days	as-cast	1040 °C 3 days
AlFe_2B_2	66.6 wt.%	97.7 wt.%	69.8 wt.%	89.3 wt.%	71.5 wt.%	100 wt.%
a (Å)	2.929(1)	2.926(4)	2.929(3)	2.925(6)	2.928(7)	2.924(1)
b (Å)	11.036(9)	11.034(0)	11.036(9)	11.030(3)	11.036(1)	11.029(9)
c (Å)	2.868(9)	2.870(1)	2.868(7)	2.864(8)	2.868(3)	2.866(0)
FeB	20.1 wt.%	2.3 wt.%	14.6 wt.%	Not detected	11.1 wt.%	Not detected
a (Å)	5.513(7)	5.513(2)	5.515(8)		5.515(4)	
b (Å)	2.949(6)	2.949(4)	2.950(1)		2.949(0)	
c (Å)	4.060(2)	4.058(6)	4.060(7)		4.059(9)	
$\text{Al}_{13}\text{Fe}_4$	13.3 wt.%	Not detected	15.6 wt.%	10.7 wt.%	17.4 wt.%	Not detected
a (Å)	15.493(5)		15.489(1)	15.500(8)	15.490(4)	
b (Å)	8.097(3)		8.095(8)	8.051(4)	8.085(8)	
c (Å)	12.506(6)		12.500(8)	12.590(0)	12.495(2)	
β	108.18(4)°		108.03(4)°	108.45(3)°	107.89(4)°	

Table 2

The value of the magnetization of alloys with initial composition of $\text{Al}_{1.0}\text{Fe}_2\text{B}_2$, $\text{Al}_{1.1}\text{Fe}_2\text{B}_2$, and $\text{Al}_{1.2}\text{Fe}_2\text{B}_2$ as-cast and annealed at 1040 °C for 3 days; expected contributions at 400 K and 50 K from ferromagnetic FeB are shown based on combination of XRD and magnetization data

Initial (nominal) composition of alloy	Magnetization at 50 K in 20 kOe (emu/g)		Magnetization at 400 K in 20 kOe (emu/g)		FeB content in as-cast alloys and expected contribution at 400 K estimated from XRD data		Curie temperature of annealed alloy (K)
	as-cast	annealed	as-cast	annealed	FeB content	contribution from FeB (emu/g)	
$\text{Al}_{1.0}\text{Fe}_2\text{B}_2$	70.7	76.7	14.6	1.85	20.1	15.0	293
$\text{Al}_{1.1}\text{Fe}_2\text{B}_2$	70.0	70.5	9.9	1.17	14.6	10.9	282
$\text{Al}_{1.2}\text{Fe}_2\text{B}_2$	68.3	68.7	6.5	1.29	11.1	8.3	282
FeB	95.6	-	74.9	-	-	-	590